IOP Publishing New J. Phys. 17 (2015) 073022 doi:10.1088/1367-2630/17/7/073022

New Journal of Physics

The open access journal at the forefront of physics

Deutsche Physikalische Gesellschaft DPG

IOP Institute of Physics

Published in partnership with: Deutsche Physikalische Gesellschaft and the Institute of Physics

OPEN ACCESS

RECEIVED
31 March 2015

REVISED
17 June 2015

ACCEPTED FOR PUBLICATION
22 June 2015

PUBLISHED
15 July 2015

PAPER

Geometrically controlled ratchet effect with collective vortex motion

V Rouco[1], A Palau[1], C Monton[2], N Del-Valle[3], C Navau[3], A Sanchez[3], X Obradors[1] and T Puig[1]

[1] Institut de Ciència de Materials de Barcelona, CSIC, Campus de la UAB, 08193 Bellaterra, Spain

[2] Department of Physics, Center for Advanced Nanoscience, University of California, San Diego, 9500 Gilman Drive, La Jolla, California 92093, USA

[3] Grup d'Electromagnetisme, Departament de Física, Universitat Autònoma de Barcelona, 08193 Bellaterra, Barcelona, Spain

E-mail: palau@icmab.es

Keywords: superconducting devices, Brownian motion, superconducting films and low-dimensional structures, transport processes vortex matter, antidots

Abstract

Rectified flux motion arising from the collective effect of many interacting vortices is obtained in a specially designed superconducting device. Ratchet structures with different asymmetric pinning potentials are generated by tuning the size, depth, and distribution of triangular blind-antidots in a high-temperature superconducting film. We experimentally and theoretically demonstrate that the amplitude and sign of the rectified vortex motion can be finely tuned with the pattern geometry. Two different dynamical regimes depending on the nature of vortices initiating the dissipation are identified, which can control the rectified vortex motion.

Single particles in an asymmetric potential show a ratchet effect, biasing or rectifying their motion, when subjected to non-equilibrium fluctuations [1–3]. The fundamental properties of ratchets have been studied in very different types of particles such as colloidal suspensions [4, 5], molecules [6], electrons [7] or quantized magnetic flux in superconductors [8–11]. Controlled motion of particles is important to provide deeper understanding of several microscopic ratchet systems and they are potentially useful for many novel electronic and molecular devices such as rectifiers, pumps, switches or transistors [12, 13].

In the case of controlled transport of magnetic flux quanta, the density and size of particles (vortices) as well as the strength of their interaction can be tuned with two external controllable parameters, i.e. temperature, T, and magnetic field, H. Ratchet effects in these systems are intimately related to the assymetry of vortex pinning arrays. Several studies have shown that besides vortex pinning effects, inter-particle interactions strongly affect vortex dynamics, giving rise to a rich phenomenology of the rectified response. Drift reversals are observed when multiple interacting particles are moving in the ratchet potential, which can depend on the magnetic field, temperature, and AC frequency [9, 10, 14, 15] or even transverse rectification effects [15, 16]. In general, in these systems the vortex dynamics is determined by the motion of a few interacting particles, since the ratchet effect disappears at high fields, whereas the study of systems containing many particles and their collective interaction is much less explored and may significantly change the transport properties from the few-particles case.

High-temperature superconductors (HTS) show a very rich H–T vortex phase diagram, making them ideally suited for the study of collective vortex interactions and dynamical flow phases in complex ratchet systems with numerous vortices. Collective effects in guided vortex motion were observed in HTS systems with triangular blind-antidots [17]. However, tailoring the ratchet vortex pinning potential to control the polarity and amplitude of rectified vortex motion in systems with many interacting particles has not been achieved until now. In this paper, we construct a system in which collective interactions on ratchets with many vortices can be manipulated through geometry controlled asymmetric pinning potentials that may provide a route to explore new implementations of ratchets in solid state devices. The robust features of net flux of a large number of particles (vortices) are observed in YBCO films with ratchet pinning potentials created by triangular blind-antidots, where both the polarity and amplitude of the rectified effect can be entirely controlled with the geometry of the patterns, instead of by external parameters such as magnetic field, temperature or frequency, as in most of the ratchet systems studied. Our ratchet device presents rectified motion up to high fields and different vortex dynamic regimes are identified depending on the rectification polarity.

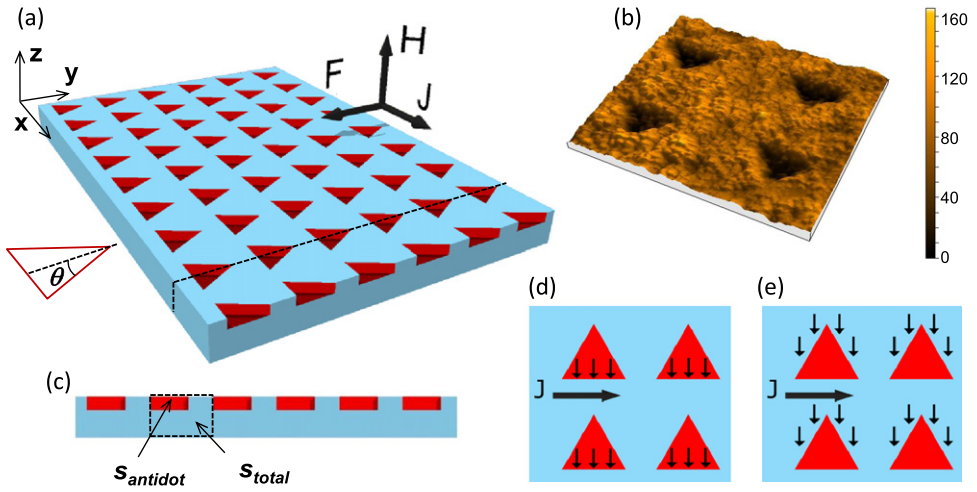

Figure 1. (a) Schematic representation of a YBCO bridge patterned with an array of triangular blind-antidots. (b) AFM image showing the surface topography of a $8 \times 8\,\mu m^2$ area of one of the patterned bridges. (c) Cross-section at the dashed line shown in (a)). The area occupied by blind-antidots is indicated in red whereas the unit area of unpatterned cross-section is indicated with a dashed line. Schematic drawings of vortex motion in a system with (d) positive and (e) negative rectification when positive current and magnetic field are applied.

High-quality epitaxial $YBa_2Cu_3O_{7-x}$ (YBCO) 250 nm thick films were grown on single-crystalline $LaAlO_3$ substrates by using a metalorganic decomposition methodology based on the trifluoroacetate precursor route [18]. Transport bridges of 100 μm in length and 20–40 μm in width were patterned in the standard four-probe configuration by optical lithography. Asymmetric potentials were generated on the bridges by patterning arrays with different size, depth, and distribution of triangular blind-antidots via focus ion beam (FIB) and electron beam lithography (EBL). In the former, a direct local etching of antidot array was obtained with the FIB Ga^+ ions whereas for the EBL we performed a wet etching of a patterned PMMA resist layer with orthophosforic acid. For all samples the pattern was designed keeping one side of the triangles along the current bridge and the other two forming an angle θ with the driving force, thus producing an asymmetry along the vortex motion direction (see figure 1(a)). The patterning conditions were optimized to avoid any damaging of the YBCO layer and good values of critical temperature, $T_c = 89$–92 K, and critical current density, $J_c\,(77\text{K}) = 2$–4 MAcm^{-2} were obtained in all the samples. Figure 1(b) shows an atomic force microscopy (AFM) micrograph of one of the patterned YBCO bridges with a blind-antidot lattice of triangles with a lateral size of 1 μm and 70 nm in depth. In-field electrical transport measurements were carried out in a quantum design PPMS. Current–voltage (I–V) curves were measured by using the standard four-probe method with the magnetic field applied perpendicular to the film plane.

Rectified vortex motion in our ratchet superconducting systems has been evaluated by inverting the direction of the driving force ($\vec{J} \times \vec{B}$) along the asymmetric pinning potential, created by the triangular array of antidots, and determining the critical current density difference at which the vortices start to move (dissipate) in each configuration. The potential is asymmetric across the transport bridge (i.e. along the $\vec{y}$ direction shown in figure 1(a)) thus we apply positive and negative dc current along $\vec{x}$ and determine the values of J_c, which we refer as J_c^+ and J_c^-, respectively. Figure 2(a) shows the difference between J_c^+ and J_c^-, $\Delta J_c = J_c^+ - J_c^-$, obtained as a function of the magnetic field for three samples with different triangular arrays of blind-antidots. For sample A1, A2 and A3 we patterned 70 nm deep blind-antidots where the sizes of triangles along the x and y directions were 3×3, 2×1.4 and $1 \times 0.85\,\mu m^2$, separated 5×5, 6×2.5 and $2.5 \times 2.5\,\mu m^2$, respectively. The value of ΔJ_c has been normalized to the value of J_c obtained at zero applied field, J_c^{sf}, such that we are able to compare net rectification effects in systems with different J_c^{sf} values. For all patterned films we observe a clear difference between J_c^+ and J_c^-, confirming the existence of a hard vortex moving direction induced by the asymmetric pinning landscape. No difference between J_c^+ and J_c^- at any value of the magnetic field were observed on unpatterned samples. Remarkably, the strength of the normalized ratchet effect, i.e. the maximum rectified critical current density, $\Delta J_c^{max}/J_c^{sf}$, changes when comparing arrays with different geometry and also their sign can be reversed (as observed in sample A3). This hints that the steepness and sign of the potential barrier that determines the hard moving direction can be modulated with the specific geometry of the pattern. It is convenient to define a dimensionless parameter as:

$$S_{\text{red}}\,(\%) = 100\frac{s_{\text{antidot}}}{s_{\text{total}}}\cos(\theta), \tag{1}$$

where s_{antidot} is the maximum area of blind-antidots perpendicular to the current flow (red area in figure 1(c)), s_{total} the cross-section area of the unpatterned bridge (dashed squared area in figure 1(c)) and θ the angle

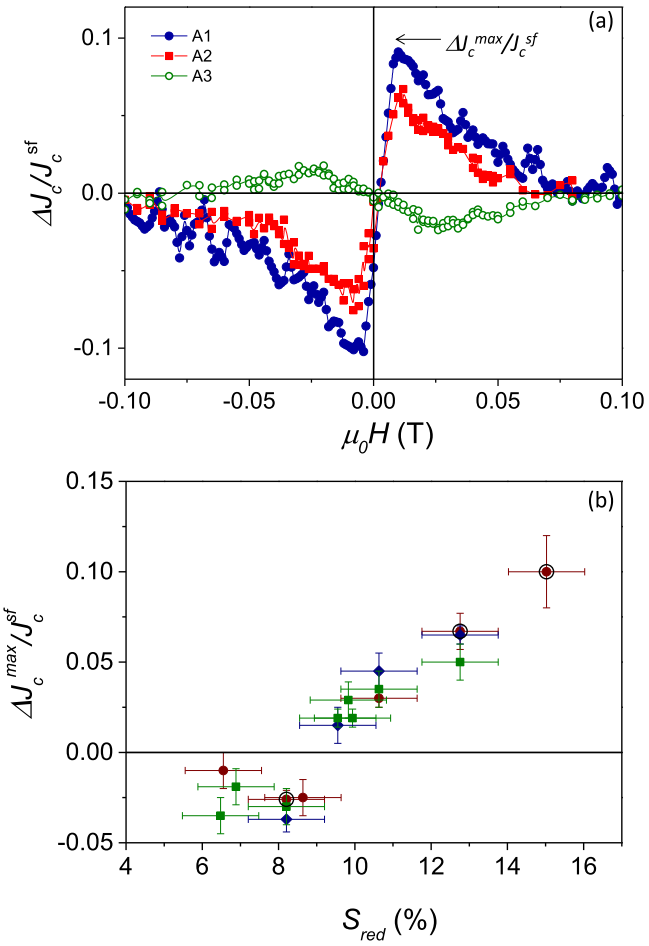

Figure 2. (a) Normalized rectification of J_c at 77 K as a function of the magnetic field for samples A1, A2 and A3 (described in the text). (b) Maximum value of $\Delta J_c/J_c^{sf}$ as a function of the S_{red} parameter for different systems at 77 K (circles), 65 K (squares) and 50 K (diamonds). Samples shown in (a) are identified with black circles.

between the tilted edges of the triangle and the driving force direction. This parameter, which considers the maximum area reduction of the current cross-section due to the presence of blind-antidots, and the asymmetry introduced by the triangular shape will help us to understand the rectified flux flow observed in our systems.

Considering equation (1) and for the particular geometry of samples A1, A2 and A3 we obtain $S_{red} = 15$, 12.7 and 8.2 respectively. So, according to this parameter, the samples with higher S_{red} values present a positive rectification (given that positive corresponds to $J_c^+ > J_c^-$ for positive applied magnetic fields), whereas the sample with negative rectification (A3) presents a lower value of S_{red}.

Figure 2(b) displays the strength of the ratchet effect, determined by the normalized maximum J_c rectification at positive magnetic fields, as a function of the S_{red}, for several systems containing different arrays of triangles, including measurements performed at various temperatures (77, 65 and 50 K). A direct correlation between the strength of the rectified vortex motion and the S_{red} value of the patterned bridges can be observed. This correlation is essentially temperature independent within the range studied, thus showing that the amplitude and direction of the ratchet effect, determined by the steepness and sign of the asymmetric potential barrier, is mainly controlled by the geometry of patterned antidots. It is important to note that there is a crossover value of $S_{red} \sim 9$ which separates the systems with positive and negative current rectification, producing therefore a geometrically controlled ratchet reversal. These experimental results indicate that the final current cross-section of the patterned bridge, characterized by S_{red}, must be the key parameter determining the sign and the amplitude of the ratchet rectification.

Although a complete modeling of the system would require full 3D simulations, a simplified 2D model can explain the effect of the geometry on the J_c rectification effect. Consider an infinitely long superconducting bar that contains several U-shaped notches (also infinitely long, simulating the blind-antidots). The calculation is based on assuming that the superconductor is in the critical state with a critical-current density depending on the local magnetic field through a Kim-type descending function [19, 20] $J_c(|H|) = J_{c0}/(1 + |H|/H_0)$, where H is the local field, $J_{c0} = 10^{11}$ A/m^2 and $\mu_0 H_0 = 0.1$T. We will assume that dissipation is first produced where the

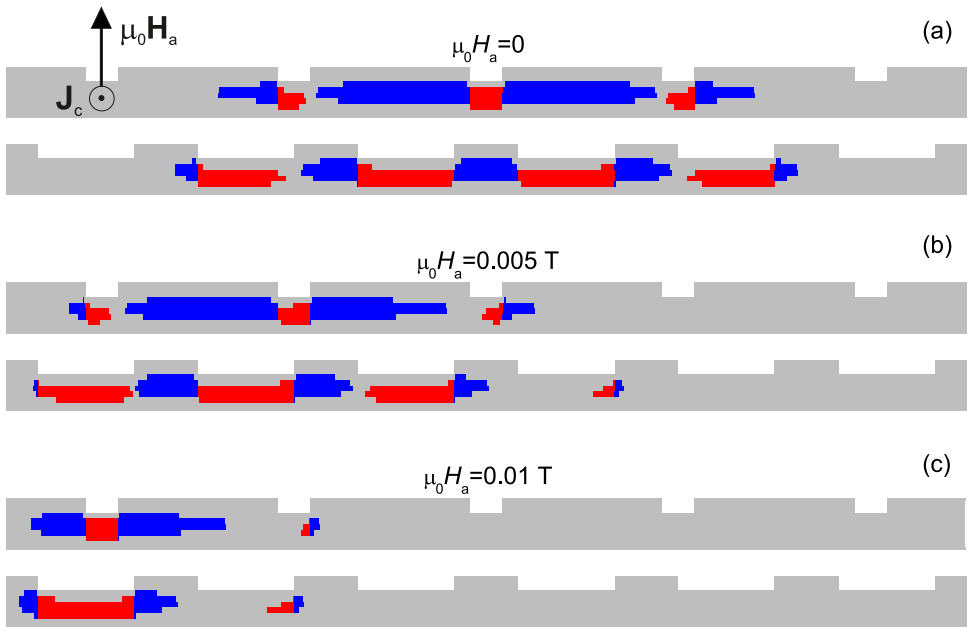

Figure 3. Calculated current density regions in long strips with two different sets of notches for different applied fields: (a) 0*T*, (b) 0.005*T* and (c) 0.01*T*. The sketch of (a) indicates the current flow and applied field directions. Colours indicate the regions with different values of current density: grey indicates $J_c < 0.95J_{c0}$, and blue and red indicate $J_c \geqslant 0.95J_{c0}$ for regions outside and below notches, respectively. The overall dimensions for the strips are 30 μm long $\times$ 250 nm thick. In the strips with five and six notches, these have widths of 1 and 3 μm, respectively. All notches have a depth of 75 nm (vertical scale is enlarged for clarity).

current density reaches its maximum value J_{c0}. For this purpose, we calculate if these dissipative regions start either below the blind-antidots or in the space between them. To quantify it, we discretize the superconductor in $N \times M$ rectangular elements (see figure 3). Starting with a constant critical current density J_k at each k-element and using an iterative procedure assuming that Biot–Savart law and the above $J_c(|H|)$ relation are satisfied, we find the critical-current density distribution all through the section of the superconductor. As a criterion, we consider that the dissipative regions are those in which the current density is above $0.95J_{c0}$. In figure 3 we show how, depending on the size of the notches, maximum dissipative areas are located either in some notched regions, driven by a vortex within the antidots (internal vortices) or outside them, driven by vortices located between the antidots (external vortex). The asymmetry observed in the dissipation areas (figures 3(b) and (c)) is due to the asymmetry of the z-component of the field created by the SC. This self-field compensates for the applied field in the left part of the SC shifting the largest values of J_c also to the left [19, 20]. Although this model, being symmetric with respect to the direction of the current flow, does not account for the ratchet effect, it is consistent with the fact that the two regimes of dissipation appear. This result points out that by changing the geometry (i.e. cross-section) of the ratchet system in a proper way one can tune the nature (internal or external) and amount of vortices initiating the dissipation. Once the dissipation is set, the sign and strength of the ratchet effect will present two different regimes. Positive rectification occurs when flux motion is induced by internal vortices. In this case, for J_c^+ and positive magnetic field, internal vortices are flowing against the base of the triangles (figure 1(d)), requiring a higher driving force than necessary to go against to the tilted edges, when the current polarity is reversed (for J_c^-), and thus $\Delta J_c > 0$. The other type of system with negative rectification, happens when motion is initiated by external vortices, which feel the opposite asymmetry of the pinning potential, rectifying the motion along the opposite direction (figure 1(e)). More complex numerical simulations considering the presence of these two types of vortices initiating the dissipation in asymmetric pinning sites [21–23] would be required in order to quantitatively describe the observed ratchet effect.

We can now go a step further in this analysis and study the flux dynamics in our collective ratchet systems when dissipation is produced either by internal or external vortices. Vortex velocities have been evaluated by measuring the voltage drop across the bridge, $V = lBv$, with B the magnetic flux density, v the average vortex velocity and l the distance between voltage contacts. The rectification of vortex motion is characterized by the difference in measured voltage for a fixed value of dc current flowing in the positive and negative x direction, $\Delta V = V^+ - V^-$. We used the maximum value of J_c (J_c^- or J_c^+ depending on the ratchet system) to determine the difference in measured voltage.

Figure 4(a) shows a contour plot of ΔV as a function of the applied magnetic field for several samples with different S_{red} values at 77 K. The upper and lower panels show ratchet systems with positive and negative J_c

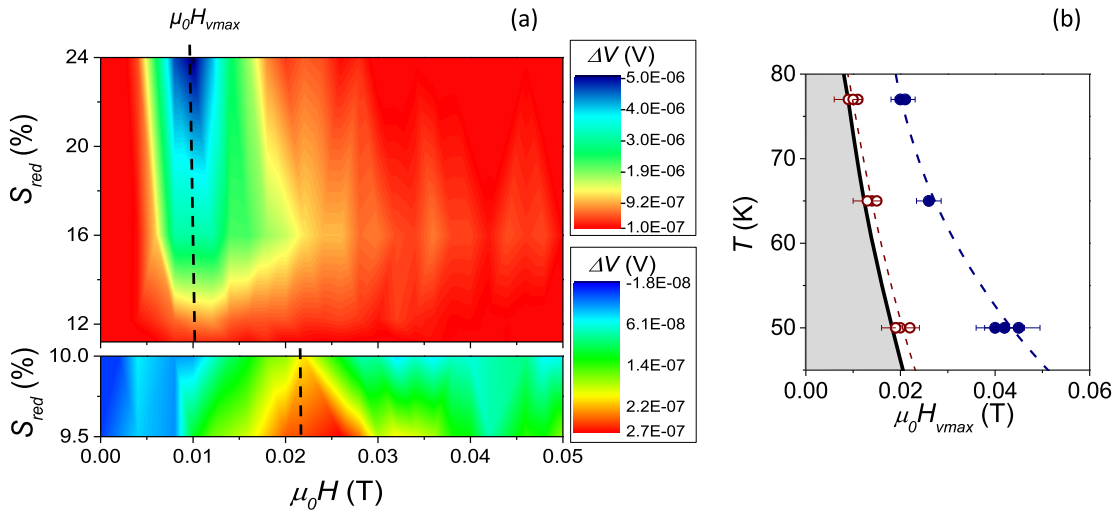

Figure 4. (a) Contour plot of the difference in measured voltage ($\Delta V = V^+ - V^-$) as a function of the magnetic field and the S_{red} value at 77 K, for systems with positive and negative rectification (upper and lower panels, respectively). (b) Magnetic field value where the maximum rectified voltage occurs as a function of the temperature for systems with positive (red open symbols) and negative rectification (blue closed symbols). Grey area corresponds to the region dominated by single-vortex pinning effects while white area corresponds to a region where vortex–vortex and vortex–defect interactions strongly compete.

rectification, respectively. It is worth noting that the maximum rectified vortex velocity (proportional to ΔV) increases as the value of S_{red} in the system is enhanced/reduced for samples presenting positive/negative rectification, in agreement with an enhancement of the ratchet strength, as shown in figure 2(b). Interestingly, the magnetic field at which the rectified vortex velocity, Δv, is maximized ($\mu_0 H_{vmax}$) only depends on the ratchet type. For systems with positive rectification we find $\mu_0 H_{vmax} \sim 0.01T$, whereas for ratchet systems with negative rectification the maximum occurs at higher fields $\mu_0 H_{vmax} \sim 0.022T$ (dashed lines in figure 4). The average number of vortices per triangle, n, at the values of the magnetic field where we find maximum rectification, are $n \sim$ 4–35 and $n \sim$ 10–100 for systems with positive and negative rectification, depending on the triangle size. These results strongly suggest that different interaction mechanisms are responsible for rectified flux flow in systems governed by internal and external vortex motion.

Figure 4(b) shows the temperature dependence $\mu_0 H_{vmax}$ for systems with positive (red open symbols) and negative (blue closed symbols) rectification. The grey region in the graph corresponds to a low-field region of single-vortex pinning where J_c is nearly independent of field and vortices mainly interact individually with the different defects present in the sample (either intrinsic or artificial). At higher fields (white region), collective effects start to be important and vortex matter enters in a regime in which vortex–vortex and vortex–defect interactions start to compete [24–26]. It is worth noting that for systems with positive rectification (driven by internal vortex motion), the maximum rectified effect occurs at lower magnetic fields than for those with negative rectification (governed by external vortex motion). In the latter case, maximum effects are obtained deep inside the region where vortex–defect interactions strongly compete with collective effects. Based on these observations one can figure out that the nature of the vortex initiating the dissipation has a significant role in the dynamics of the ratchet effect. Systems with negative rectification require strong vortex–vortex interactions to work. This kind of ratchet may be described if one assumes that external vortices do not directly interact with the asymmetric blind-antidots but they feel the asymmetric pinning potential through collective interactions with internal pinned vortices within the triangles [17, 27]. Conversely, for systems with positive rectification, the field range where maximum effect is obtained appears in a region with weak vortex–vortex interactions and thus in this case it is reasonable to assume that collective interactions are not essencial to generate the ratchet potential. The asymmetry in this case would come from the nano-wall pinning created at the edges of the blind triangles [28].

In conclusion, we have demonstrated geometrically controlled rectified vortex motion effects in YBCO films patterned with asymmetric triangular blind-antidots. In these systems, both the steepness and sign of the ratchet potential can be tailored with the geometry (size, depth, and distribution) of the patterned triangles. Geometrically inverse rectification effects can be well described by numerical simulations considering the final cross-section of patterned bridges. Two different vortex dynamic regimes have been identified in positive and negative rectification systems. In the former, ratchet effects are determined via direct interaction between vortices and asymmetric patterns. In the latter, the ratchet dynamics is mainly governed by strong collective vortex interactions. Using a system based on a high-temperature superconductor we are able to explore the

physics of ratchet systems with many interacting vortices, providing a useful toolbox for controlling and manipulating transport of multiple particles at the nanoscale. In these systems, the sign of rectified effects does not show any temperature or field dependence but is fixed by the structure geometry.

Acknowledgments

This work has been supported by MINECO (MAT2014-51778-C2-1R, MAT2012-35370, CSD2007-0041, IPT-2011-1090-920000), Generalitat de Catalunya (SGR2014-00753, 2014SGR150, XaRMAE), EU-FP7 NMP-LA-2012-280432 EUROTAPES project and Cost Action MP1201. VR acknowledges the JAE-CSIC PhD grant. AS acknowledges funding from an ICREA Academia award.

References

[1] Feynman R P, Leighton R B and Sands M 1963 *The Feynman Lectures on Physics* vol I (Reading, MA: Addison-Wesley) ch 46
[2] Astumian R D 1997 Thermodynamics and kinetics of a brownian motor *Science* **276** 917–22
[3] Astumian R D and Hanggi P 2002 Brownian motors *Phys. Today* **55** 33–39
[4] Rousselet J, Salome L, Ajdari A and Prostt J 1994 Directional motion of brownian particles induced by a periodic asymmetric potential *Nature* **370** 446–8
[5] Matthias S and Muller F 2003 Asymmetric pores in a silicon membrane acting as massively parallel brownian ratchets *Nature* **424** 53–57
[6] van Oudenaarden A and Boxer S G 1999 Brownian ratchets: molecular separations in lipid bilayers supported on patterned arrays *Science* **285** 1046–48
[7] Linke H, Humphrey T E, Lofgren A, Sushkov A O, Newbury R, Taylor R P and Omling P 1999 Experimental tunneling ratchets *Science* **286** 2314–7
[8] Lee C S, Janko B, Derenyi I and Barabasi A L 1999 Reducing vortex density in superconductors using the ratchet effect *Nature* **400** 337–40
[9] Villegas J E, Savelev S, Nori F, Gonzalez E M, Anguita J V, Garca R and Vicent J L 2003 A superconducting reversible rectifier that controls the motion of magnetic flux quanta *Science* **302** 1188–91
[10] de Souza Silva C C, de Vondel J V, Morelle M and Moshchalkov V V 2006 Controlled multiple reversals of a ratchet effect *Nature* **440** 651–4
[11] Plourde B L T 2009 Nanostructured superconductors with asymmetric pinning potentials: vortex ratchets IEEE Trans *Appl. Supercond.* **19** 3698–7
[12] Savel'ev S and Nori F 2002 Experimentally realizable devices for controlling the motion of magnetic flux quanta in anisotropic superconductors *Nat. Mater.* **1** 179–84
[13] Hanggi P and Marchesoni F 2009 Artificial Brownian motors: controling transport on the nanoscale *Rev. Mod. Phys.* **81** 387–440
[14] Gillijns W, Silhanek A V, Moshchalkov V V, Olson Reichhardt C J and Reichhardt C 2007 Origin of reversed vortex ratchet motion *Phys. Rev. Lett.* **99** 247002
[15] Olson C J and Reichhardt C 2005 Rectification and flux reversals for vortices interacting with triangular traps *Physica* C **432** 125–32
[16] Wordenweber R, Dymashevski P and Misko V R 2004 Guidance of vortices and the vortex ratchet effect in high-t-c superconducting thin films obtained by arrangement of antidots *Phys. Rev.* B **69** 184504
[17] Palau A, Monton C, Rouco V, Obradors X and Puig T 2012 *Phys. Rev.* B **85** 0125021–5
[18] Obradors X, Puig T, Ricart S, Coll M, Gazquez J, Palau A and Granados X 2012 Growth, nanostructure and vortex pinning in superconducting YBCO thin films based on trisolutions *Supercond. Sci. Technol.* **25** 123001
[19] Sanchez A, Navau C, Del-Valle N, Chen D-X and Clem J R 2010 Self-fields in thin superconducting tapes: implications for the thickness effect in coated conductors *Appl. Phys. Lett.* **96** 072510
[20] Del-Valle N, Navau C, Sanchez A and Dinner R B 2012 Transport critical-current density of superconducting films with hysteretic ferromagnetic dots *AIP Adv.* **2** 022166
[21] Zhu B Y, Marchesoni F, Moshchalkov V V and Nori F 2003 Controllable step motors and rectifiers of magnetic flux quanta using periodic arrays of asymmetric pinning defects *Phys. Rev.* B **68** 014514
[22] Zhu B Y, Marchesoni F and Nori F 2004 Controlling the motion of magnetic flux quanta *Phys. Rev. Lett.* **92** 180602
[23] Savel'ev S, Misko V, Marchesoni F and Nori F 2005 Separating particles according to their physical properties: transverse drift of underdamped and overdamped interacting particles diffusing through two-dimensional ratchets *Phys. Rev.* B **71** 214303
[24] Aytug T, Paranthaman M, Leonard K J, Kang S, Martin P M, Heatherly L, Goyal A, Ijaduola A O, Thompson J R and Christen D K 2006 Analysis of flux pinning in YBCO films by nanoparticle-modified substrate surfaces *Phys. Rev.* B **74** 184505
[25] Zuev Y L, Christen D K, Wee S H, Goyal A and Cook S W 2008 Near-isotropic performance of intrinsically anisotropic high-temperature superconducting tapes due to self-assembled nanostructures *Appl. Phys. Lett.* **93** 172512
[26] Palau A, Bartolome E, Llordes A, Puig T and Obradors X 2011 Isotropic and anisotropic pinning in TFA-grown YBCO films with BZO nanoparticles *Supercond. Sci. Technol.* **24** 125010
[27] Olson C J, Reichhardt C, Janko B and Nori F 2001 Collective interaction-driven ratchet for transporting flux quanta *Phys. Rev. Lett.* **87** 177002
[28] Palau A, Rouco V, Luccas R F, Obradors X and Puig T 2014 Nanowall pinning for enhanced pinning force in YBCO films with nanofabricated structures *Physica* C **506** 178–83